cmgh
CELLULAR AND MOLECULAR GASTROENTEROLOGY AND HEPATOLOGY

ORIGINAL RESEARCH

Mitogen-activated Protein Kinase Kinase Activity Maintains Acinar-to-Ductal Metaplasia and Is Required for Organ Regeneration in Pancreatitis

Christopher J. Halbrook,[1,2] Hui-Ju Wen,[1,2] Jeanine M. Ruggeri,[1,2] Kenneth K. Takeuchi,[1,2] Yaqing Zhang,[3] Marina Pasca di Magliano,[3] and Howard C. Crawford[1,2]

[1]Department of Molecular and Integrative Physiology, [2]Department of Internal Medicine, and [3]Department of Surgery, University of Michigan, Ann Arbor, Michigan

SUMMARY

Mitogen-activated protein kinase kinase signaling is required for initiation and maintenance of pancreatitis. Inhibition of this signaling pathway attenuates inflammation and fibrosis, but also limits organ regeneration.

BACKGROUND & AIMS: Mitogen-activated protein kinase (MAPK) signaling in the exocrine pancreas has been extensively studied in the context of pancreatic cancer, where its potential as a therapeutic target is limited by acquired drug resistance. However, its role in pancreatitis is less understood. We investigated the role of mitogen-activated protein kinase kinase (MEK)-initiated MAPK signaling in pancreatitis to determine the potential for MEK inhibition in treating pancreatitis patients.

METHODS: To examine the role of MEK signaling in pancreatitis, we used both genetic and pharmacologic approaches to inhibit the MAPK signaling pathway in a murine model of cerulein-induced pancreatitis. We generated mice harboring inducible short hairpins targeting the MEK isoforms *Map2k1* and/or *Map2k2* specifically in the pancreatic epithelium. We also used the MEK inhibitor trametinib to determine the efficacy of systemic inhibition in mice with pancreatitis.

RESULTS: We demonstrated an essential role for MEK signaling in the initiation of pancreatitis. We showed that both systemic and parenchyma-specific MEK inhibition in established pancreatitis induces epithelial differentiation and stromal remodeling. However, systemic MEK inhibition also leads to a loss of the proliferative capacity of the pancreas, preventing the restoration of organ mass.

CONCLUSIONS: MEK activity is required for the initiation and maintenance of pancreatitis. MEK inhibition may be useful in the treatment of chronic pancreatitis to interrupt the vicious cycle of destruction and repair but at the expense of organ regeneration. *(Cell Mol Gastroenterol Hepatol 2016;■:■–■; http://dx.doi.org/10.1016/j.jcmgh.2016.09.009)*

Keywords: Inflammation; Wound Healing; Tissue Regeneration; ADM.

Pancreatitis is the most frequent cause for hospitalization for a gastrointestinal disease.[1] Repeated bouts of acute pancreatitis cause a necrosis-fibrosis sequence leading to chronic pancreatitis (CP), which is characterized by progressive and potentially irreversible damage to the pancreas.[2] Although some acinar cells are lost during pancreatitis through necrosis,[3] other acinar cells undergo acinar-to-ductal metaplasia (ADM).[4] ADM are proliferative duct-like structures theoretically capable of regenerating acinar cells lost in pancreatitis.[4–6] ADM induction has been linked to several mechanisms including ductal ectasia,[7] activation of nuclear factor kappa B (NF-κB),[8,9] Notch receptors,[10,11] and epidermal growth factor receptor (EGFR). Activation of EGFR by ectopic ligands has been demonstrated to drive ADM in ex vivo cultures[10,12] and in vivo.[12,13]

High levels of RAS activity, established through transgenic overexpression of oncogenic *Kras,* are sufficient to drive CP and ADM.[14] This effect is mediated through RAS activation of NF-κB signaling, which propagates a feed-forward signaling loop promoting chronic inflammation.[15] We and others have demonstrated that endogenously expressed mutant *Kras* requires EGFR to achieve sufficient RAS activity to induce ADM and tumorigenesis.[16,17] We also observed that pharmacologic inhibition of mitogen-activated protein kinase kinase (MEK) is sufficient to block KRAS-driven ADM and subsequent tumor formation,[17] whereas MEK inhibition of established pancreatic intraepithelial neoplasia induces acinar cell redifferentiation.[18] Taken together, these data strongly support a key role for *KRAS-MEK* signaling in the formation and maintenance of pancreatic preneoplasia.

In contrast to tumorigenesis, the role of mitogen-activated protein kinase (MAPK) signaling in the induction

Abbreviations used in this paper: **ADM, acinar-to-ductal metaplasia; BrdU, bromodeoxyuridine; CP, chronic pancreatitis; EGFR, epidermal growth factor receptor; MAPK, mitogen-activated protein kinase; MEK, mitogen-activated protein kinase kinase; NF-κB, nuclear factor kappa B; pERK, phosphorylated extracellular signal–regulated kinase; qRT-PCR, quantitative reverse transcriptase–polymerase chain reaction; sh, short hairpin; WT, wild-type.**

2352-345X
http://dx.doi.org/10.1016/j.jcmgh.2016.09.009

and persistence of pancreatitis in the absence of oncogenic *Kras* is less well-elucidated. Pancreatitis is marked by an influx of macrophages that can release cytokines such as tumor necrosis factor-α and RANTES driving ADM by activation of NF-κB.[8] In addition, alternatively activated macrophages promote the activation of pancreatic stellate cells, further enhancing the fibroinflammatory response.[19] It has been postulated that stromally derived cytokines and growth factors are primarily responsible for driving acinar cell damage and ADM.[8] However, expression of EGFR ligands and EGFR activation is commonly observed in human CP, and in mice, parenchymal ablation of either EGFR or ADAM17, the primary EGFR ligand sheddase, prevents ADM and the stromal response in a cerulein model of pancreatitis.[17] These data collectively suggest that MEK signaling in epithelial cells, downstream of EGFR activation, is required for initiation of pancreatitis, including ADM and the fibroinflammatory response. The possibility that MEK activity is important for maintaining ADM suggests that MEK inhibitors may offer a treatment strategy for CP in human patients, for which there currently are no effective alternatives.[2]

Here we have determined that inhibition of MAPK signaling in cerulein-induced pancreatitis by treatment with the MEK inhibitor trametinib blocked CP development. Furthermore, short-term trametinib treatment of established pancreatitis restored exocrine tissue and dramatically reduced inflammation and fibrosis. However, inhibition of MEK interfered with the restorative capacity of the organ by blocking cell proliferation. With longer-term trametinib treatment, loss of organ regeneration was even more pronounced. By using short hairpin (sh) RNA mouse models individually targeting both major MEK isoforms, we found that parenchyma-specific knockdown of MEK blocked pancreatitis-induced ADM and the associated inflammation and fibrosis. Together, these data show that MEK signaling is a potent driver of the overall pancreatitis phenotype and is required for limited organ regeneration.

Results

Blockade of Mitogen-activated Protein Kinase Signaling Prevents Chronic Pancreatitis

Previously we showed that parenchymal EGFR and its activation by ADAM17 are required for pancreatic tumorigenesis,[17] attributing this effect to a reduction in downstream MEK activation. We also found that parenchymal ablation of EGFR or ADAM17 blunted all aspects of experimental pancreatitis.[17] However, in each of these models, EGFR signaling was chronically inhibited before disease onset, preventing us from examining acute effects. Here we set out to explore the feasibility of acute MEK inhibition as a potential treatment for CP. First, we performed immunohistochemistry for phosphorylated extracellular signal–regulated kinase (pERK) on a human pancreas tissue microarray that included normal and CP samples (Figure 1*A*) to determine whether MEK activity is potentially relevant to human CP. Ten of 12 CP samples showed pERK positivity in the epithelia and 12 of 12 in stromal cells. In contrast, 2 of 56 normal pancreas samples showed pERK positivity in the epithelia and 4 of 56 in the stroma. This ERK activity may be a result of being normal tissue in close proximity to cancer.

Pancreatitis can be induced in mice by administration of supramaximal doses of cerulein, a cholecystokinin ortholog, with the extent of damage determined by the amount and duration of treatment. Mild treatment regimens induce symptoms of acute pancreatitis, marked by acinar cell necrosis and an innate immune response. A more severe treatment protocol results in a phenotype more reminiscent of human CP, marked by ADM, fibrosis, and innate and adaptive immune responses.[17] However, unlike human CP, damage induced by chronic cerulein treatment resolves over time after cerulein withdrawal.

To investigate whether systemic inhibition of MEK blocked cerulein-induced pancreatitis in a manner similar to EGFR gene ablation, we pretreated mice with either the MEK inhibitor trametinib (T-CP) or vehicle (V-CP) and then continued this treatment with a cerulein treatment regimen that elicits a CP-like phenotype (Figure 1*B*) or saline as a vehicle control. The efficacy of trametinib treatment was verified by immunoblotting tissue lysates harvested from V-CP and T-CP groups, where ~60% lower pERK levels were observed (Figure 1*C*).

Histologic examination of pancreas tissue demonstrated that cerulein treatment strongly induced a dropout of acinar tissue and a gain of fibrotic stroma (Figure 1*D*). V-CP mice had ~70% loss of acinar cell area, defined by area positive for amylase by immunohistochemistry (Figure 1*E*), compared with saline controls. Loss of acinar cells was accompanied by gain of a picrosirius-positive fibrotic stroma (Figure 1*F*), rich in inflammatory cells. Pancreata from T-CP animals had dramatically more amylase-positive acinar tissue compared with vehicle control, as well as significantly less fibrosis. The fibroinflammatory response and acinar dropout correlated to organ atrophy associated with CP, with V-CP pancreata losing 60% of their relative pancreatic mass compared with saline control (Figure 1*G*). In contrast, T-CP mice lost only 35% of relative pancreas mass compared with saline control. There were no apparent differences in the tissue of mice treated with trametinib or vehicle in the absence of cerulein (Figure 1*H*).

To support the histologic findings, RNA was harvested from the tissue of V-CP and T-CP mice. Quantitative reverse transcriptase–polymerase chain reaction (qRT-PCR) was performed to assess the acinar vs ductal composition of the pancreas (Figure 1*I*). As expected, levels of amylase (Amy2b) were dramatically higher and levels of the ductal marker cytokeratin 19 (Krt19) were significantly lower in T-CP pancreata vs V-CP pancreata. Transcripts for the acinar-specific transcription factors Ptf1a and Mist1 confirmed higher levels of acinar differentiation in T-CP mice compared with V-CP mice.

Consistent with the epithelial response, examination of immune cell infiltration in the cerulein-treated tissue (Figure 1*J* and *K*) revealed that trametinib treatment strongly attenuated F4/80$^+$ macrophage, Ly6b.2$^+$

neutrophil, and CD-3^{+} T-cell influx compared with vehicle treatment. Trametinib treatment also dramatically reduced the conversion of isolated acinar cell explants embedded in Matrigel (Corning, Corning, NY) to ductal cysts compared with vehicle control (Figure 1*L* and *M*), suggesting that the effects of MEK inhibition are at least in part due to effects of the inhibitor on ADM, independent of inflammation.

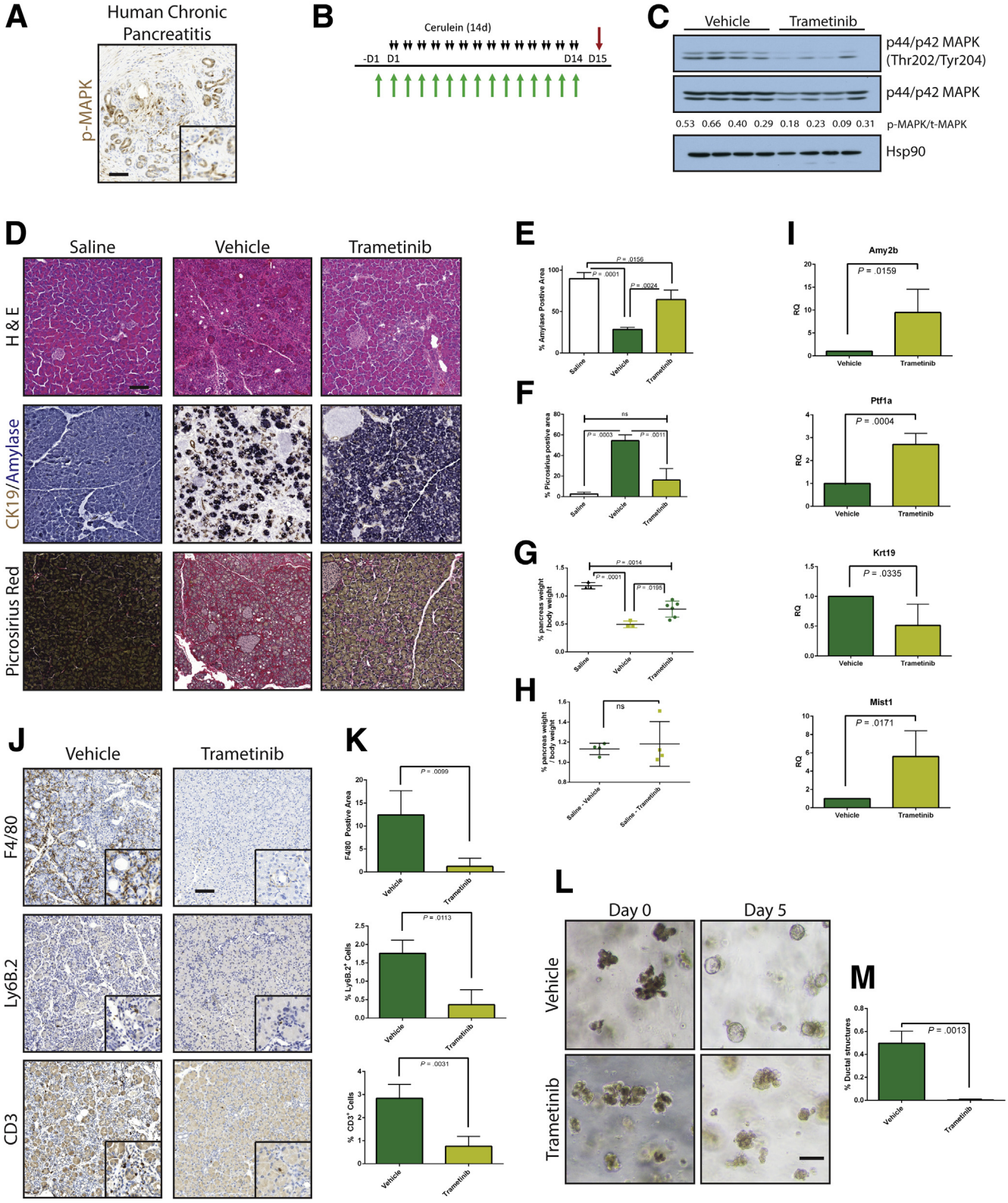

Mitogen-activated Protein Kinase Kinase 1 and Mitogen-activated Protein Kinase Kinase 2 Isoforms Are Redundant in Pancreatitis

The systemic use of trametinib cannot distinguish between the contributions of the individual MEK1 and MEK2 isoforms or between parenchymal and stromal activities. MEK1 and MEK2 have been shown in several other systems to have some non-redundant functions,[20–25] and we found prominent ERK activity in both the epithelial and stromal compartments in human CP (Figure 1*A*). To more precisely dissect the contributions of the MEK proteins, we generated mice in which we could conditionally and independently knock down expression MEK1 and MEK2 isoforms in vivo. Mice containing shRNAs targeting *Map2k1* or *Map2k2* (shMEK1, shMEK2) were cloned under the control of a Tet operator and knocked in downstream of the Col1A1 locus. These mice were crossed with mice harboring a Cre-dependent tetracycline transactivator in a background with the pancreas-specific Ptf1a$^{Cre/+}$. The shMEK1 and shMEK2 lines were also interbred to allow simultaneous knockdown of both MEK isoforms (Figure 2*A*). Doxycycline-induced expression of shRNAs resulted in an effective knockdown of the targeted isoform with no cross reactivity, whereas the shMEK1/2 mice demonstrated a loss of expression of both isoforms (Figure 2*B*). Potent knockdown of the target MEK isoform was observed with 72 hours of doxycycline treatment, with the greatest level of knockdown achieved with 1 week of treatment (Figure 2*C*). The specificity of the shRNA expression was confirmed to be confined to the pancreas of mice harboring all the required transgenes by fluorescent imaging (Figure 2*D*). Importantly, there was no discernible effect on the normal pancreas from the knockdown of any of the genes or the expression of a control shRNA targeting *Renilla* luciferase (shRen713) (Figure 2*E*).

To test the requirement of MEK isoforms on the induction of CP, shRNA and Ptf1a$^{+/Cre}$ control mice were treated chronically with cerulein after activation of shRNA expression (Figures 3 and 4). Knockdown of either MEK1 or MEK2 alone was indistinguishable from wild-type (WT) and non-target shRNA control mice, in which the tissue was heavily damaged after cerulein treatment (Figure 3*B*). However, the knockdown of both MEK1 and MEK2 together revealed potent inhibition of MAPK activation (Figure 4*B*) and led to a significant retention of acinar cell mass, as well as a marked decrease in the amount of fibrosis and significant reduction in immune infiltration (Figure 4*C*–*E*), similar to trametinib treatment.

In line with these histologic observations, knockdown of MEK1/2 led to dramatically higher transcript levels of acinar differentiation markers as well as decreased Krt19 levels (Figure 4*F*) and was able to efficiently block the transdifferentiation of Matrigel-embedded acinar cells to ductal cysts (Figure 4*G* and *H*). Consistent with the results from trametinib treatment, a significant difference was seen in the relative pancreatic mass between cerulein-treated shMEK1/2 mice as compared with rttA controls (Figure 4*I*).

Mitogen-activated Protein Kinase Kinase Inhibition Does Not Block Acute Damage

We had previously observed that EGFR is required for CP induction but not for the acute cerulein response,[17] demonstrating that the blockade with chronic treatment was not due to trivial effects on cerulein signaling. It has also been suggested that MAPK inhibition mitigates the acute effects of cerulein-induced pancreatitis.[26] To test whether either trametinib treatment or knockdown might be affecting cerulein signaling itself, we examined the effect of MEK blockade on acute pancreatitis. Mice were pretreated with trametinib or vehicle as before and then concurrently with a cerulein regimen that would induce acute pancreatitis (Figure 5*A*). The acute cerulein treatment resulted in several hallmarks of acute pancreatitis including edema, necrosis, and an increase in serum amylase (Figure 5*B* and *C*) regardless of inhibitor treatment. The shRNA mice and control mice were treated with doxycycline and subjected to the same acute pancreatitis protocol (Figure 5*D*). After similar trametinib treatment, cerulein-treated shMEK1/2 mice showed necrosis and edema and demonstrated no difference in serum amylase levels compared with cerulein-treated shRNA or control mice (Figure 5*E* and *F*). These data indicate the initial response of the acinar compartment to cerulein is not blocked by MEK inhibition through either systemic or parenchymal-specific means.

Figure 1. (***See previous page***). MEK inhibition can block the onset of CP. (*A*) Immunohistochemistry for phosphorylated MAPK in human pancreatitis samples. (*B*) CP protocol with drug pretreatment. *Black arrows* indicate cerulein injection; *green arrows* indicate vehicle or trametinib treatment. (*C*) Immunoblot for levels of phosphorylated MAPK, total MAPK, and the loading control HSP90. The ratio of the band intensities of phosphorylated/total MAPK is indicated under each lane. (*D*) Histologic characterization of tissue remodeling, hematoxylin-eosin staining (H&E), dual immunohistochemistry with ductal marker CK19 (*brown*) and acinar marker amylase (*blue*), and picrosirius red stain, with respective quantitation (*E* and *F*) n $\geq$ 3 for all groups. *White* indicates saline treated; *green* indicates vehicle + cerulein; *yellow* indicates trametinib + cerulein. (*G*) Relative pancreas mass, defined by percentage pancreas weight over body weight, n = 3 for saline and vehicle, n = 6 for trametinib. (*H*) Relative pancreas mass, defined by percentage pancreas weight over body weight, n = 4 for all groups. (*I*) qRT-PCR analysis of acinar markers Amy2b, Ptf1a, and Mist1 and ductal marker Krt19. (*J*) Immunohistochemistry for macrophages (F/480), neutrophils (Ly6B.2), and T-cells (CD3) with respective quantitation (*K*) n $\geq$ 3 for all groups. (*L*) Acinar cell explants embedded in Matrigel were imaged at Day 0 and Day 5. (*M*) Acinar to ductal cyst conversion on day 5 was quantitated by a blinded observer, n = 3. Scale bars = 100 μm for all panels, 50 μm for insets. Error bars represent mean with standard deviation.

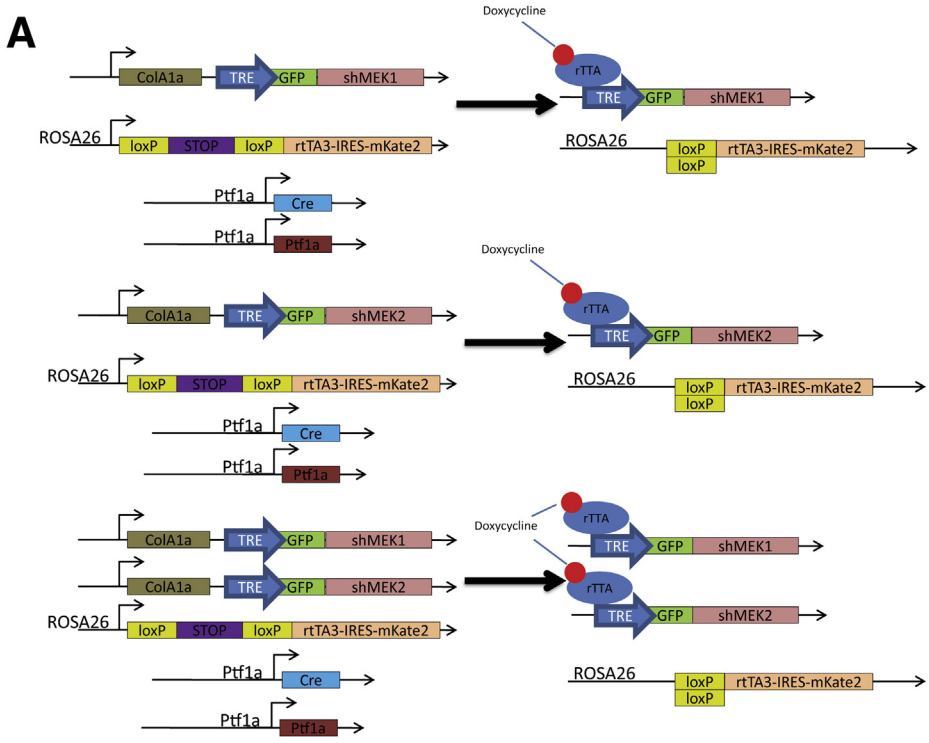
A
Doxycycline
ColA1a
TRE
GFP
shMEK1
rTTA
ROSA26
loxP
STOP
loxP
rtTA3-IRES-mKate2
Ptf1a
Cre
Ptf1a
shMEK2
shMEK1
shMEK2

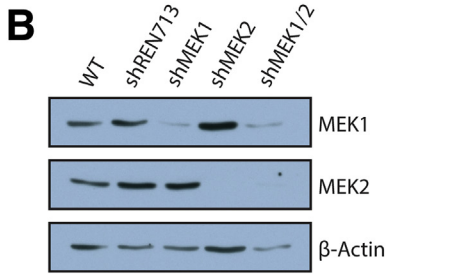
B
WT
shREN713
shMEK1
shMEK2
shMEK1/2
MEK1
MEK2
β-Actin

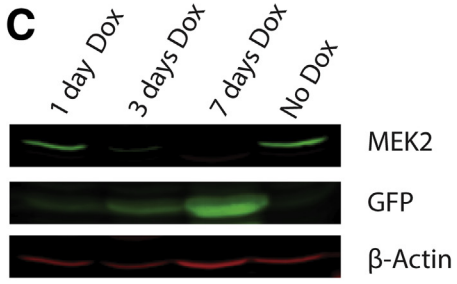
C
1 day Dox
3 days Dox
7 days Dox
No Dox
MEK2
GFP
β-Actin

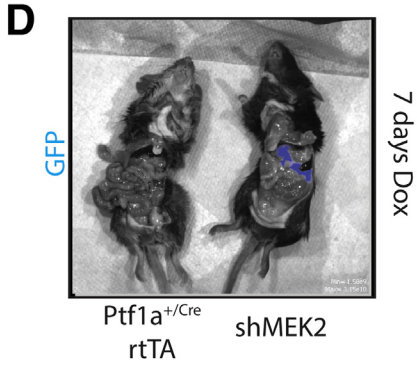
D
GFP
7 days Dox
Ptf1a+/Cre
rtTA
shMEK2

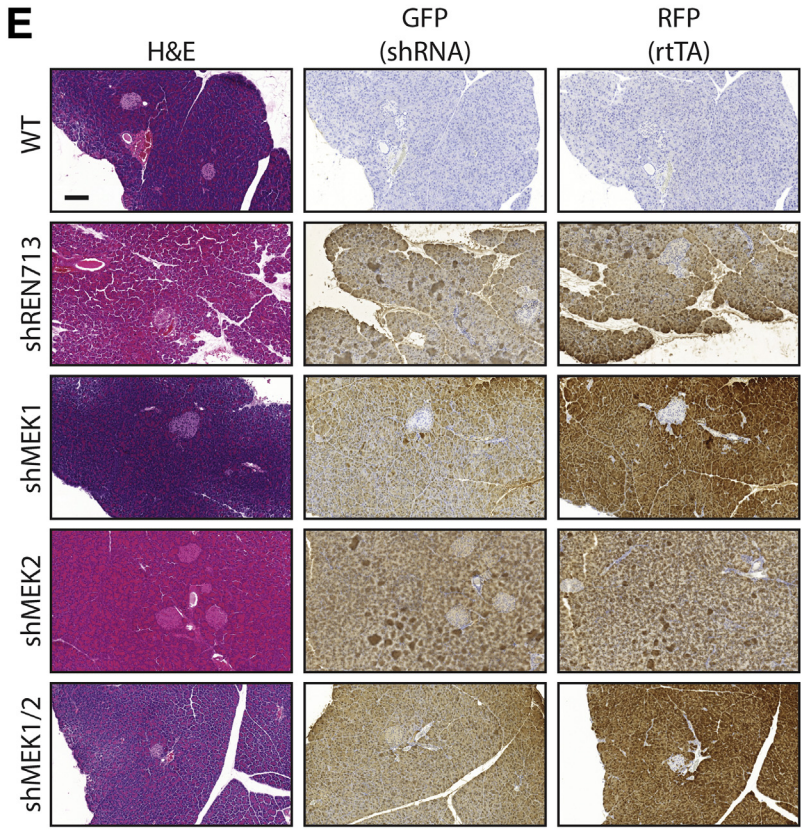
E
H&E
GFP (shRNA)
RFP (rtTA)
WT
shREN713
shMEK1
shMEK2
shMEK1/2

Systemic Inhibition of Mitogen-activated Protein Kinase Kinase Ameliorates the Pancreatitis Phenotype but Disrupts Organ Regeneration

Having established that MEK inhibition concurrent with cerulein treatment blocks the onset of the pancreatitis phenotype, we set out to test whether MEK inhibition can reverse the pancreatitis phenotype. First, we induced CP in WT mice with cerulein and then continued cerulein treatment together with either trametinib or vehicle (Figure 6*A*) or withdrew them from cerulein treatment entirely to allow recovery (Figure 6*B*). Western blotting confirmed that MAPK activation was reduced in the trametinib-treated group compared with the vehicle-treated mice (Figure 6*C*). Trametinib treatment was sufficient to restore a significant amount of acinar tissue, with 80% of the amylase-positive area compared with the recovered cohort, whereas the vehicle-treated mice had less than 50% of the recovered control (Figure 6*D* and *E*). Trametinib treatment also reduced fibrosis compared with vehicle-treated controls and dramatically lowered the number of macrophages, neutrophils, and T cells (Figure 6*D* and *F*). However, in trametinib-treated mice the relative mass of the pancreas did not reach to the same size as the recovery group (Figure 6*G*), suggesting that MEK activity was required not just for maintenance of ADM but also for the tissue regenerative function of ADM. We confirmed that trametinib treatment induced acinar cell redifferentiation by using qRT-PCR analysis for acinar cell differentiation markers, compared with vehicle-treated mice. However, transcript levels of the ductal marker Krt19 remained unchanged between the 2 groups.

Our data to this point were consistent with MEK inhibition driving the redifferentiation of acinar cells from ADM. However, ADM is known to be highly proliferative,[6] presumably contributing to the restoration of organ mass. Therefore, reversing the metaplastic state before sufficient proliferation or blocking epithelial proliferation globally regardless of differentiation status may prevent the pancreatic regeneration that would normally follow cessation of the damaging insult. To determine whether MEK inhibition blocks the proliferative capacity of the epithelium, we treated mice with cerulein for 1 week to establish a modest pancreatitis phenotype and then treated the mice with trametinib or vehicle for 48 hours to investigate the early effects of MEK inhibition. To track proliferation, bromodeoxyuridine (BrdU) was administered 4 hours before death (Figure 7*A*). Inhibition of MAPK activation was verified by Western blot (Figure 7*B*), and BrdU incorporation was measured by immunohistochemistry (Figure 7*C*). Indeed, levels of BrdU incorporation were significantly higher in vehicle-treated animals compared with trametinib-treated mice (Figure 7*D*). In addition, RNA transcript levels of several acinar markers increased while the levels of Krt19 decreased in the trametinib-treated group (Figure 7*E*), which is consistent with the hypothesis that MEK activity is required for both proliferation and maintenance of the ADM differentiation state. Further analysis by using coimmunofluorescence for Ki67, as a marker of proliferation, the acinar cell marker carboxypeptidase A, and the ductal marker CK19 revealed that proliferative capacity of both the epithelial (positive for either) and the stromal/inflammatory compartments (negative for both) was reduced by MAPK inhibition (Figure 7*F* and *G*). The consequences of anti-proliferative effects of MEK inhibition were more profound with longer-term cerulein treatment with MEK inhibition (7 days of cerulein followed by 14 days of combined cerulein and trametinib or vehicle), resulting in an even more severe loss of pancreatic mass (Figure 8).

Maintenance of Pancreatitis Requires Epithelial Mitogen-activated Protein Kinase Kinase Signaling

We next investigated whether knockdown of parenchymal MEK1 and MEK2 was sufficient to reverse the damage of established pancreatitis. Pancreatitis was established in shMEK1/2 mice by cerulein treatment. Mice were then either removed from cerulein treatment and allowed to recover or continued on cerulein treatment with and without doxycycline-induced shRNA expression (Figure 9*A*–*C*). The shRNA expressing mice treated with cerulein demonstrated significant recovery of acinar mass and decreased levels of fibrosis compared with mice lacking shRNA expression (Figure 9*D* and *E*). This was also accompanied by a loss of macrophage and neutrophil infiltration; however, there were more T cells in the mice expressing shRNA under cerulein treatment compared with the recovery group (Figure 9*F*–*H*). Inhibition of MAPK activation in the doxycycline-treated mice was verified by Western blot for pERK (Figure 9*I*), whereas the induction of expression of acinar markers and loss of Krt19 expression were verified by qRT-PCR (Figure 9*J*). No differences were seen in mice expressing a control short hairpin and in mice expressing single short hairpins targeting MEK1 or MEK2 alone. The relative pancreatic mass also did not differ between treatment groups (data not shown).

Figure 2. (***See previous page***). shRNA mouse characterization. (*A*) Representative genetic scheme of pancreas-specific inducible shRNA mice. (*B*) Western blot for MEK1, MEK2, and β-actin of protein lysate from pancreata harvested from doxycycline-treated mice. (*C*) Western blot for MEK2 expression as a function of time from shMEK2 mouse on doxycycline. (*D*) Fluorescent imaging demonstrating shRNA expression specifically in the pancreas of shRNA mice. (*E*) Histologic representation of tissue from doxycycline-treated mice. Scale bars = 200 μm. GFP, green fluorescent protein; RFP, red fluorescent protein.

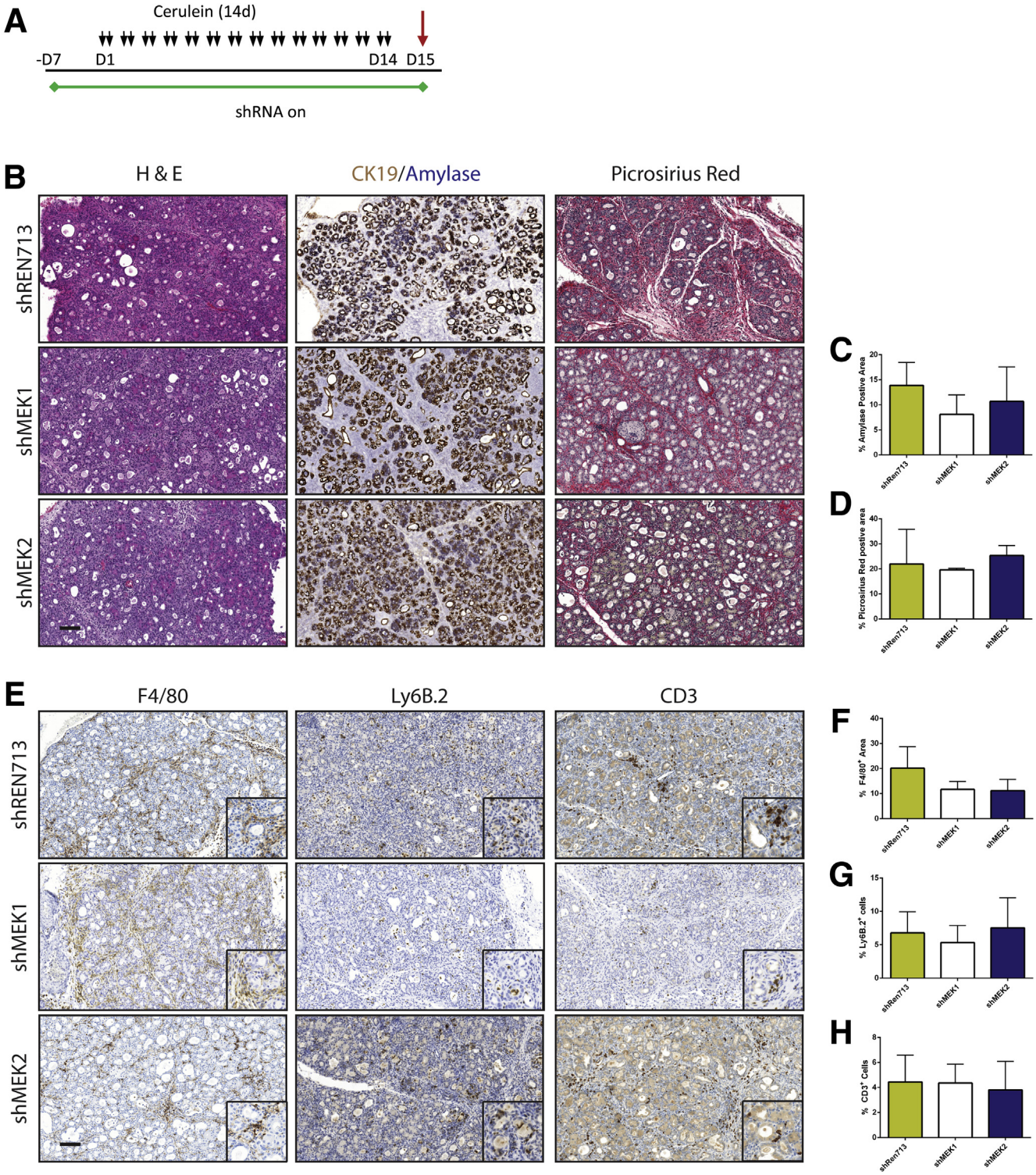

Figure 3. Knockdown of MEK1, MEK2, or non-target control has no effect on induction of CP. (*A*) Schematic representation of CP protocol after initiation of shRNA expression. (*B*) Histologic representation of tissue remodeling with respective quantitation. (*C* and *D*) n $\geq$ 3 for all groups. (*E*) Immunohistochemistry for macrophage, neutrophil, and T-cell infiltration. (*F–H*) Quantitation of respective immunohistochemistry staining; error bars represent mean with standard deviation, n $\geq$ 3 in all groups. Scale bars = 100 μm for panels, 50 μm for insets.

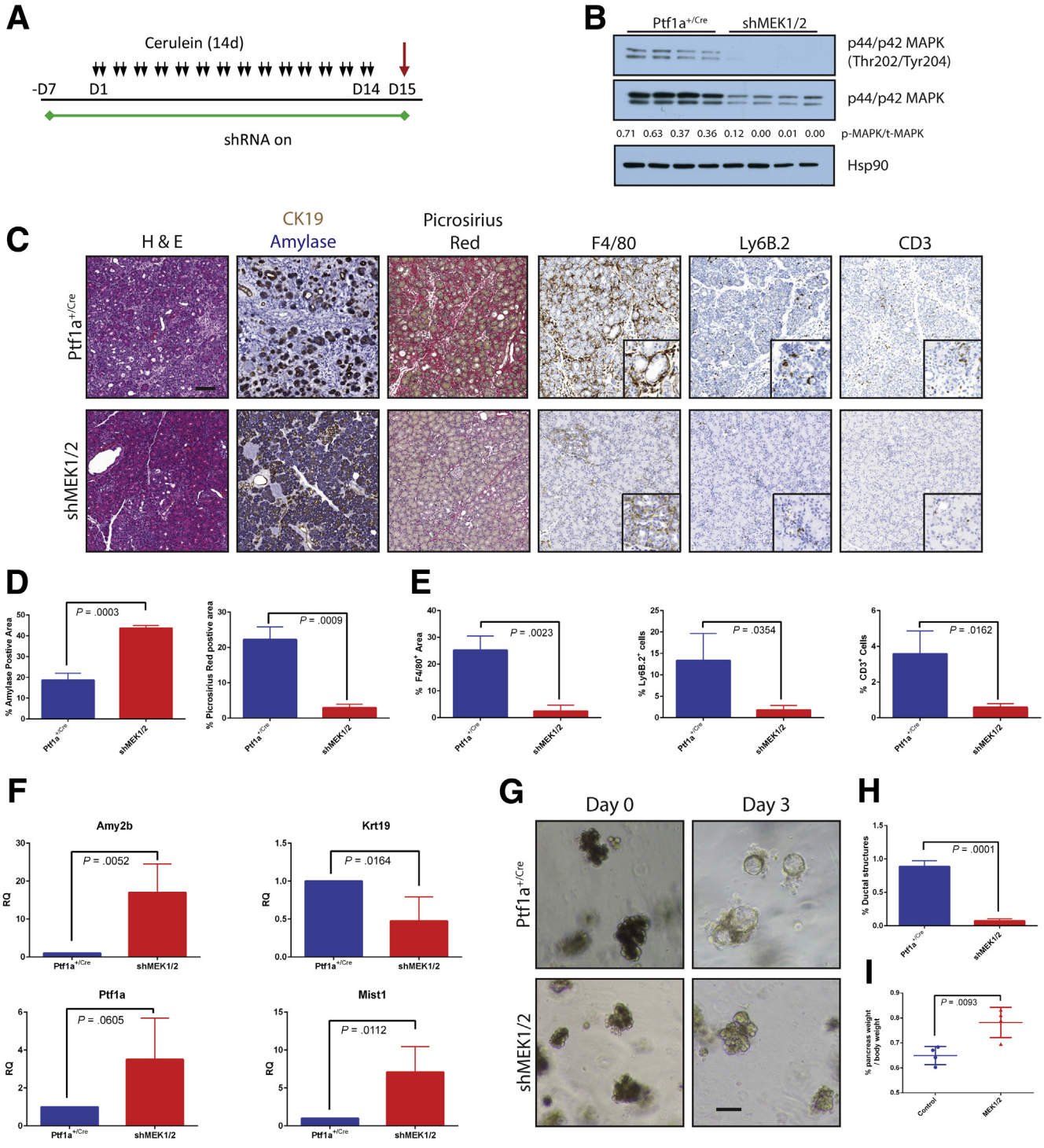

Figure 4. Combined genetic knockdown of MEK1 and MEK2 can prevent onset of pancreatitis. (*A*) CP protocol after initiation of shRNA expression. (*B*) Immunoblot for levels of phosphorylated MAPK, total MAPK, and the loading control HSP90. The ratio of the band intensities of phosphorylated/total MAPK is indicated under each lane. (*C*) Representative histology of each genotype with quantitation for amylase and picrosirius positive tissue (*D*) and immune cell infiltration (*E*). *Blue bars* represent Ptf1a$^{+/Cre}$ control mice; *red bars* indicate shMEK1/2 mice, n $\geq$ 3 for all comparisons. (*F*) qRT-PCR analysis of acinar markers Amy2b, Ptf1a, and Mist1 and ductal marker Krt19, n = 4. (*G*) Acinar cell explants embedded in Matrigel were imaged at Day 0 and Day 3. (*H*) Acinar to ductal cyst conversion on Day 3 as quantitated by a blinded observer, n = 3. (*I*) Relative pancreas mass, defined by percentage pancreas weight over body weight, n = 4 for all groups. Error bars represent mean with standard deviation. Scale bars = 100 μm for panels, 50 μm for insets.

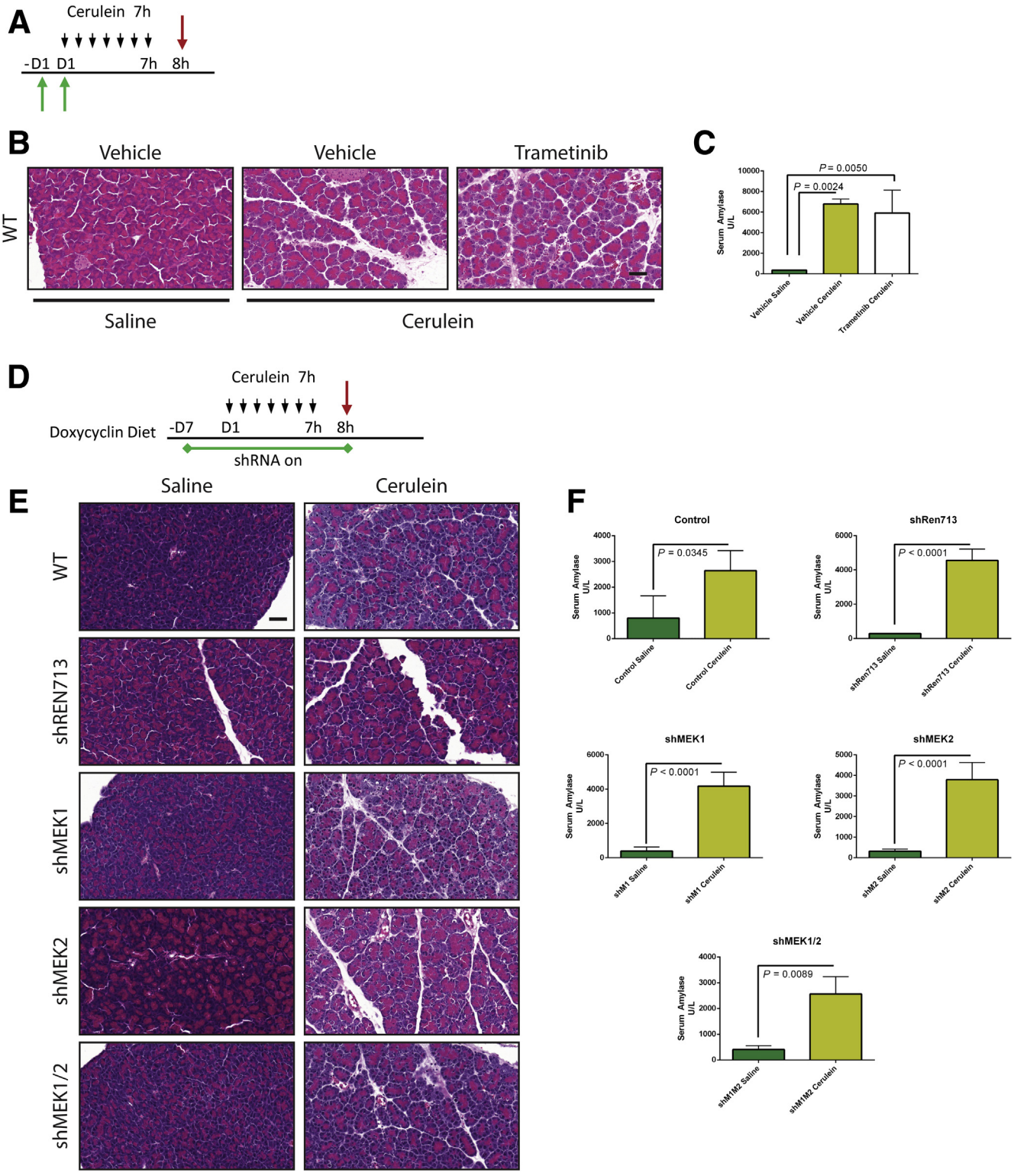

Figure 5. MEK inhibition does not block induction of pancreatitis by cerulein. (*A*) Acute pancreatitis treatment protocol after pretreatment with either MEK inhibitor or vehicle. (*B*) Representative H&E stains for each inhibitor treatment group. (*C*) Serum amylase levels for inhibitor treatments as detected by spectrophotometric activity assay. n = 3 for all groups. (*D*) Acute pancreatitis treatment protocol after activation of shRNA. (*E*) H&E stains for each shRNA treatment group. (*F*) Serum amylase levels for shRNA mice as detected by spectrophotometric activity assay. n = 3 for all groups. Scale bars = 100 μm.

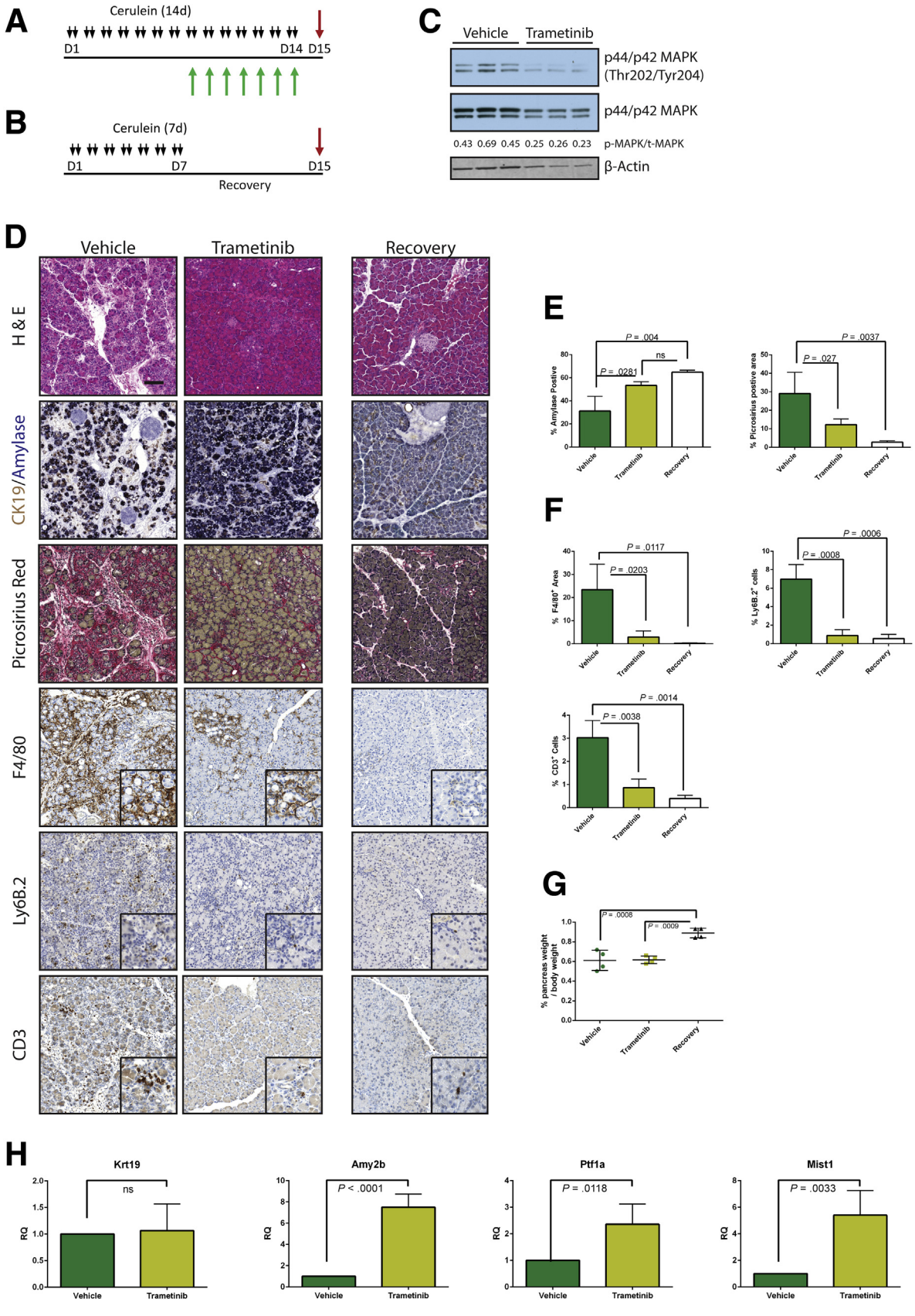
A
Cerulein (14d)
D1
D14 D15
B
Cerulein (7d)
D1
D7
D15
Recovery
C
Vehicle
Trametinib
p44/p42 MAPK (Thr202/Tyr204)
p44/p42 MAPK
0.43 0.69 0.45 0.25 0.26 0.23
p-MAPK/t-MAPK
β-Actin
D
Vehicle
Trametinib
Recovery
H & E
CK19/Amylase
Picrosirius Red
F4/80
Ly6B.2
CD3
E
P = .004
ns
P = .0281
% Amylase Positive
P = .0037
P = .027
% Picrosirius postive area
F
P = .0117
P = .0203
% F4/80+ Area
P = .0006
P = .0008
% Ly6B.2+ cells
P = .0014
P = .0038
% CD3+ Cells
G
P = .0008
P = .0009
% pancreas weight / body weight
H
Krt19
ns
RQ
Amy2b
P < .0001
Ptf1a
P = .0118
Mist1
P = .0033
Vehicle
Trametinib

Cytokine Expression Is Modulated by Mitogen-activated Protein Kinase Signaling

The observation that blocking MEK signaling affected not just the epithelium but also the resulting fibroinflammatory response led us to examine cytokine production in mice treated with cerulein plus trametinib or vehicle. Whole tissue lysate was harvested from either untreated mice or mice treated with cerulein to establish pancreatitis, then concurrently treated with cerulein in combination with trametinib or vehicle (Figure 10*A*), and then examined by using a mouse cytokine array (Figure 10*B*). Among the cytokines detected in the array, the proinflammatory cytokines CXCL1, TNF-α, MCP1, ICAM1, IL1a, IL16, IL23, CXCL12, CSF1, as well as the canonically negative regulators TIMP1 and IL1-ra, were increased in CP and downregulated by trametinib treatment. With the cytokine array results as a guide, we used qRT-PCR analysis to confirm a significant reduction in expression of many proinflammatory cytokines in mice treated with trametinib after establishment of pancreatitis (Figure 10*C*) and in mice treated with trametinib before the induction of CP (Figure 11*A*). The RNA expression levels of many of these cytokines were also suppressed in doxycycline-treated shMEK1/2 mice after the establishment of pancreatitis (Figure 10*D* and *E*) or knockdown of MEK1 and MEK2 before cerulein treatment compared with Ptf1a$^{Cre/+}$ control mice (Figure 11*B*). Together, these data suggest that MEK inhibition, either systemically or in the parenchyma, prevents the establishment of the proinflammatory cytokine-rich microenvironment that exacerbates the fibroinflammatory response associated with CP (Figure 10*F*), disrupting ADM/inflammatory cell reciprocal communication in pancreatitis.

Discussion

Pancreatitis is a serious health issue without any effective treatments. Our earlier studies on the importance of EGFR activity in pancreatic tumorigenesis strongly implicated EGFR/KRAS/MEK/ERK signaling in the very earliest stages of tumor formation,[17] including those processes also associated with CP such as ADM. Here we show that MEK signaling is required not only for the initiation of the metaplastic process and the associated fibroinflammatory response but also for maintaining the transdifferentiated, metaplastic state. These observations closely mirror data implicating MAPK signaling in both the initiation and maintenance of metaplasia in the chief cells of the stomach epithelium,[27] illustrating a commonality in the role of MAPK signaling on the plasticity of Mist1 expressing serous exocrine cells in different organs.[28] Genetic or pharmacologic inhibition of MEK activity consistently led to a larger population of amylase-positive acinar cells, decreased fibrosis, and an attenuated inflammatory response after the onset of pancreatitis. However, despite the amelioration of the common characteristics of pancreatitis pathology, chronic MEK inhibition also prevented the restoration of pancreatic mass that would be associated with legitimate healing.

It has previously been demonstrated that the MAPK signaling pathway is upregulated in response to damage and required for adaptive pancreatic growth.[29,30] Our data further suggest that the MEK-ERK signaling axis is also an important part of the pancreatic wound healing process, similar to what has been observed in the regeneration of other gastrointestinal systems. Injury to the gastric mucosa results in activation of ERK in an EGFR-dependent manner, initiating the proliferation and migration necessary to begin the wound healing process.[31,32] Furthermore, the EGFR ligand HB-EGF has also been demonstrated to play an important role in intestinal restitution after ischemia in a manner requiring both the MEK-ERK and PI3-kinase pathways downstream of EGFR signaling.[33]

The wound healing process can also be viewed in the context of tissue regeneration from a progenitor population. In *Drosophilla* EGFR-MAPK signaling is required for intestinal stem cells to regenerate the midgut epithelium after bacterial infection.[34] EGFR and Notch pathways also cooperate to initiate proliferation and differentiation of gastric stem cells in response to injury.[35] However, unlike the intestine, the pancreas lacks a confirmed adult stem cell population. The proliferative nature of ADM compared with normal acinar or duct cells, together with the ultimate recovery of an acinar cell population after experimental pancreatitis, has led to the hypothesis that ADM is involved in the limited tissue regeneration observed on resolution of the damaging insult.[4,6] However, several studies suggest other sources of restored acinar cells after injury, including proliferation of other mature acinar cells,[5] proliferation and differentiation of centroacinar cells,[36] transdifferentiation of a duct cell subpopulation,[37,38] or expansion of a rare DCLK1-positive cell population.[39] Here we show that MEK inhibition after induction of pancreatitis blocks cell division, yet it increases the relative acinar cell population, suggesting that the precursors of these new acinar cells are preexisting rather than being derived from the proliferative expansion and differentiation of a small subpopulation of cells. The

Figure 6. (***See previous page***). Trametinib treatment of established pancreatitis leads to reverse of tissue damage but not of tissue mass. CP protocol with inhibitor or vehicle treatment (*A*) or pancreatitis with recovery protocol (*B*). (*C*) Immunoblot for levels of phosphorylated MAPK, total MAPK, and the loading control β-actin. The ratio of the band intensities of phosphorylated/total MAPK is indicated under each lane. (*D*) Histologic representation of tissue remodeling and immune cell counts with quantitation (*E* and *F*, respectively), n $\geq$ 3 in all groups. *White bars* indicate the recovered cohort, *green bars* indicate cerulein + vehicle treated, and *yellow bars* indicate the cerulein + trametinib treated group. (*G*) Relative pancreas mass, defined by percentage pancreas weight over body weight, of each treatment group, n = 4 in all groups. (*H*) qRT-PCR analysis of acinar markers Amy2b, Ptf1a, and Mist1 and ductal marker Krt19, n = 3.

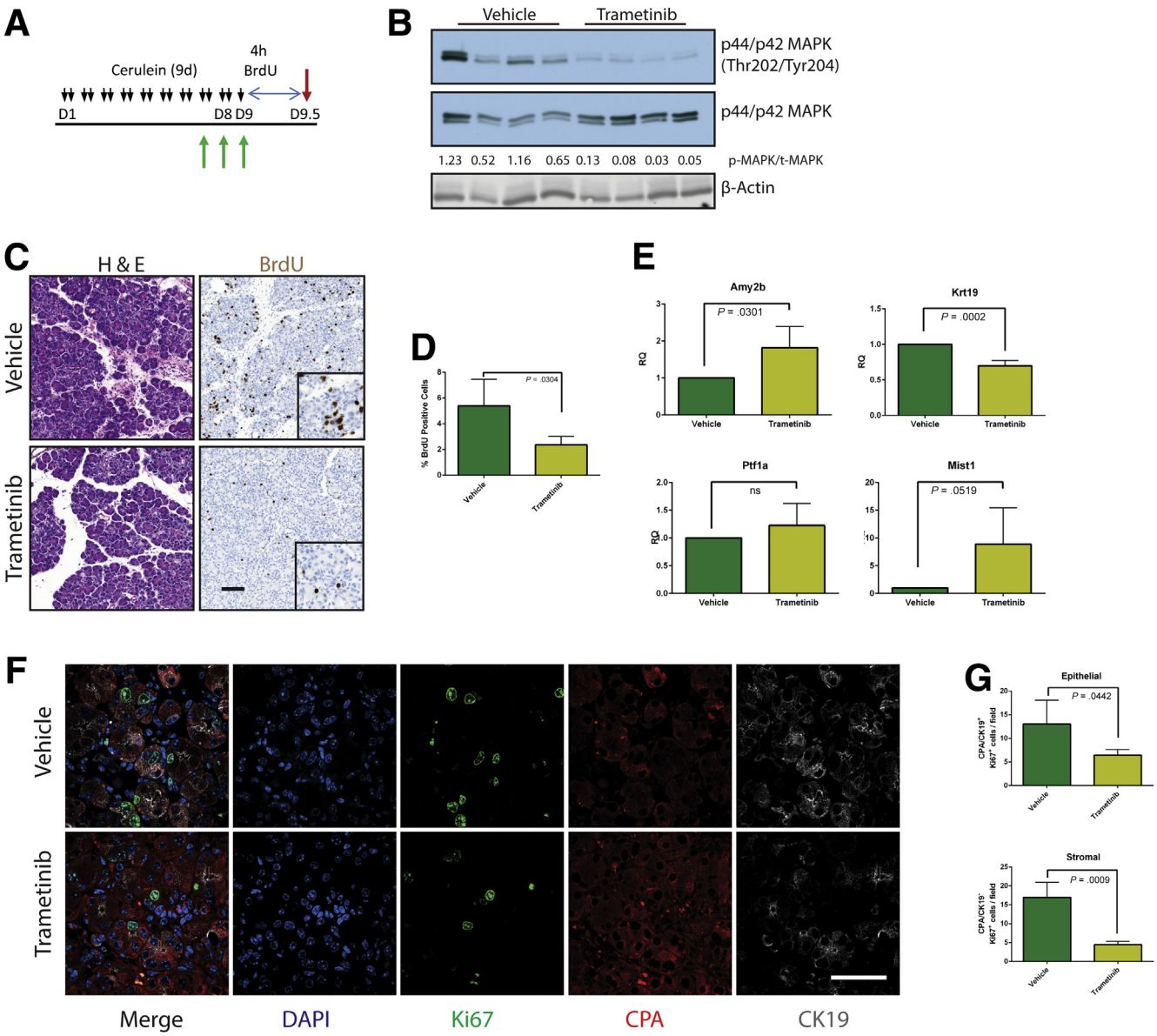

Figure 7. MEK inhibition inhibits acinar proliferation in response to tissue damage. (*A*) Abbreviated CP protocol with BrdU addition to assay proliferation. (*B*) Immunoblot for levels of phosphorylated MAPK, total MAPK, and the loading control β-actin. (*C*) Histologic representation of tissue by H&E, immunohistochemistry for BrdU incorporation, and quantitation of BrdU staining (*D*), n = 4 for both groups. (*E*) qRT-PCR analysis of acinar markers Amy2b, Ptf1a, and Mist1 and ductal marker Krt19, n = 4. (*F*) Representative immunofluorescence images for DAPI (*blue*), Ki67 (*green*), CPA (*red*), and CK19 (*white*). (*G*) Ki67 quantitated by stromal ($CPA^-/CK19^-$) or epithelial (CPA^+ and/or $CK19^+$) compartment. Error bars represent mean with standard deviation. Scale bars = 100 μm for panels, 50 μm for insets.

lack of regeneration seen in response to systemic MEK inhibition can also be, at least in part, a direct effect of MEK inhibition preventing macrophage recruitment and/or polarization, an important component of pancreatic regeneration.[40] None of these possibilities are mutually exclusive, but our data support a model where metaplastic ducts have the capacity to redifferentiate into acinar cells and that MEK activity is required for maintaining their metaplastic state.

The failure to regenerate organ mass clearly suggests a potentially deleterious consequence to MEK inhibition in treating pancreatitis. However, unlike experimental models of pancreatitis where the entire organ is simultaneously affected by the damaging agent, human CP usually manifests as a relatively localized region of sometimes severe damage and inflammation. Although MEK inhibition may prevent tissue regeneration in the afflicted region of the pancreas, we have found no adverse effects of short-term MEK inhibition on the normal pancreas. As such, the potential to resolve the pathology of the affected region, including the inflammation, without compromising the majority of the organ suggests

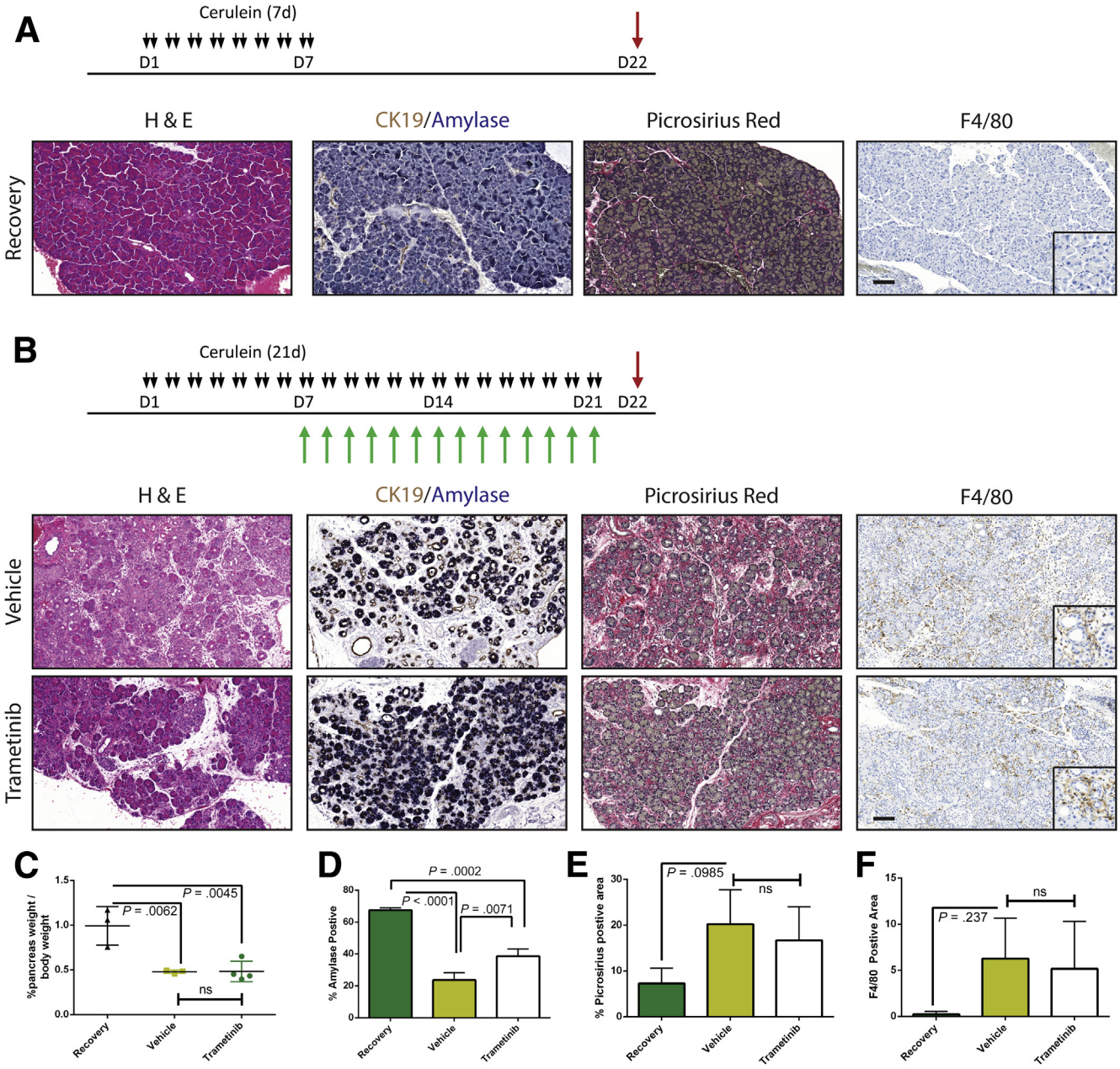

Figure 8. Long-term inhibition of MEK results in loss of ameliorative effect. Schematic representation of CP protocol with inhibitor or vehicle treatment (*A*) or pancreatitis with recovery protocol (*B*). (*C*) Relative pancreas mass of each treatment group, defined by percentage pancreas weight over body weight, n = 3 for recovery and vehicle and n = 4 for trametinib. (*D–F*) Quantitation of respective staining for each group; error bars represent mean with standard deviation, n ≥ 3 for all groups. Scale bars = 100 μm for panels, 50 μm for insets.

some promise for MEK inhibition in the treatment of pancreatitis.

Methods

Mouse Strains

Ptf1a$^{Cre/+}$ and shRen713 mice have been previously described.[41,42] The shMapk2k1 and shMap2k2 mice were generated by Mirimus Inc (Cold Spring Harbor, NY) on a mixed background and contained a ROSA26-CAG-LSL-rtTA^{3}-IRES-mKate2 reverse tetracycline transactivator.[43] WT C57BL/6 mice were obtained from Jackson Labs (Bar Harbor, ME). Cerulein treatments were performed on animals between 6 and 12 weeks of age, with doxycycline treatments started up to 1 week before treating animals with cerulein. Animal experiments were conducted in accordance with the Office of Laboratory Animal Welfare and approved by the Institutional Animal Care and Use Committees of Stony Brook University, Mayo Clinic, and the University of Michigan.

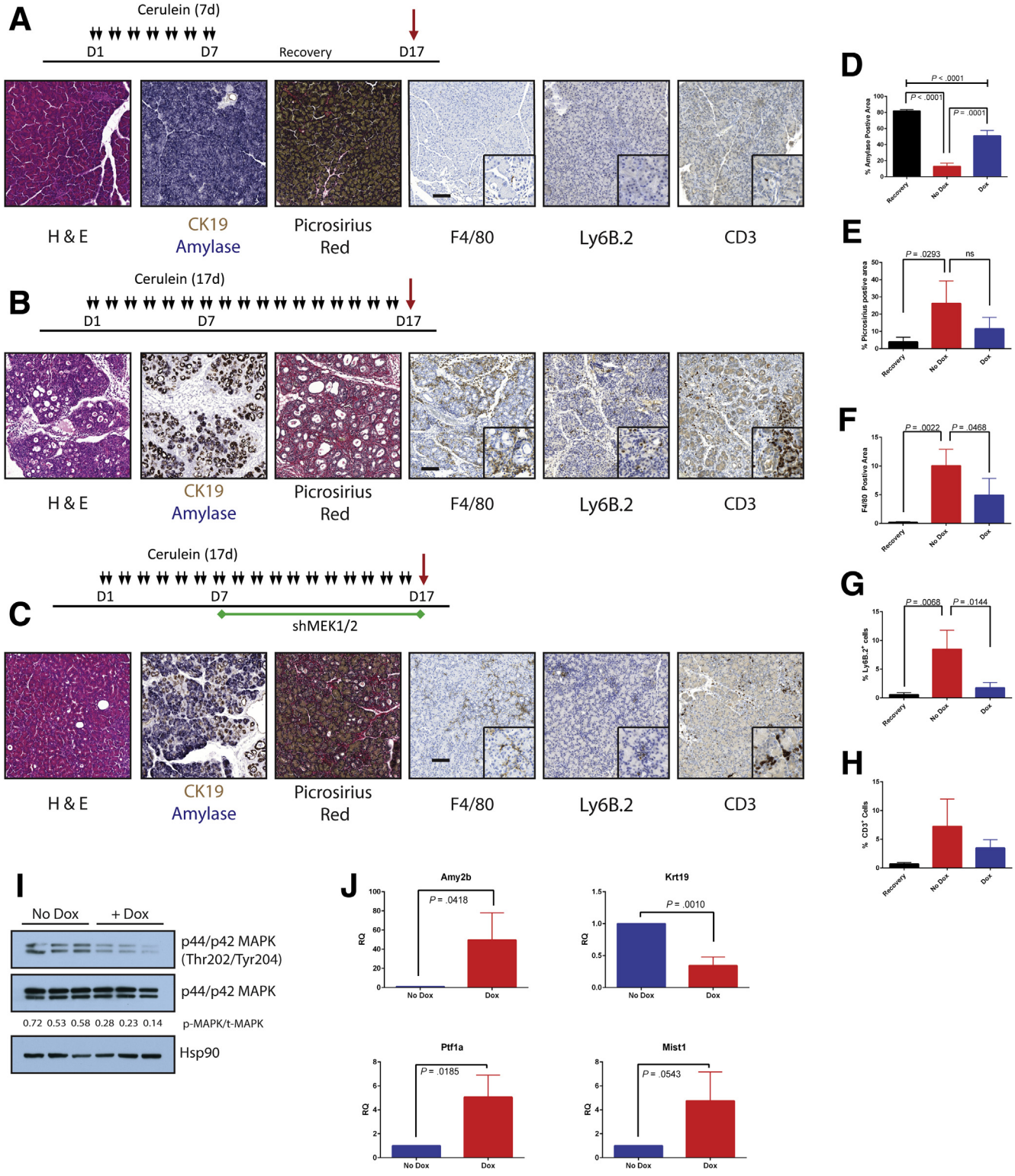

Figure 9. Combined knockdown of MEK1 and MEK2 can reverse cerulein-induced damage. Schematic and histologic representation of pancreatitis with recovery protocol (Recovery) (*A*), CP protocol (No Dox) (*B*), or shRNA activation during CP protocol (Dox) (*C*). (*D–H*) Quantitation of respective staining; error bars represent mean with standard deviation, n $\geq$ 3. (*I*) Immunoblot for levels of phosphorylated MAPK, total MAPK, and the loading control HSP90. (*J*) qRT-PCR analysis of acinar markers Amy2b, Ptf1a, and Mist1 and ductal marker Krt19; n = 3. Scale bars = 100 μm for panels, 50 μm for insets.

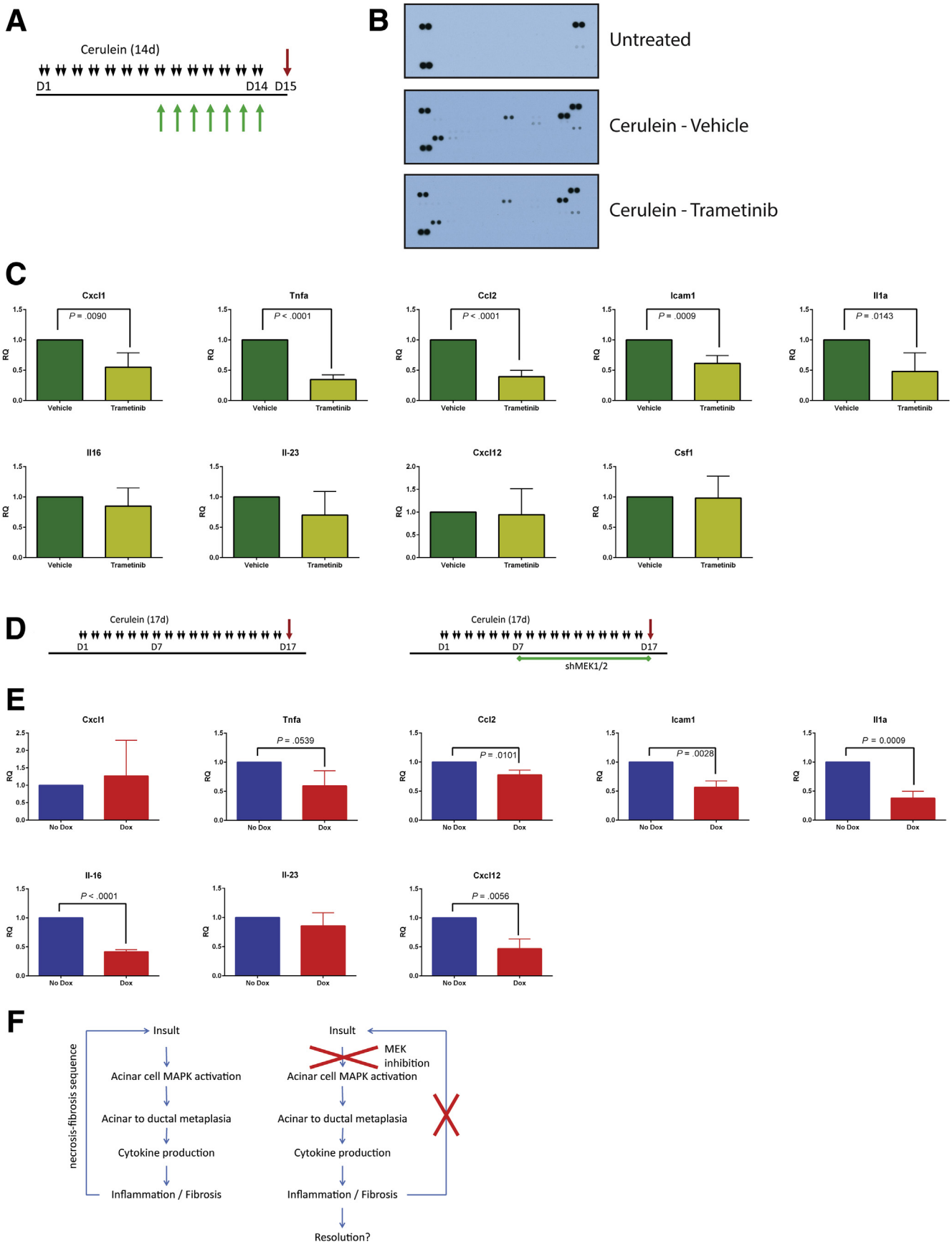
A
Cerulein (14d)
D1
D14
D15
B
Untreated
Cerulein - Vehicle
Cerulein - Trametinib
C
Cxcl1
P = .0090
Tnfa
P < .0001
Ccl2
P < .0001
Icam1
P = .0009
Il1a
P = .0143
Il16
Il-23
Cxcl12
Csf1
RQ
Vehicle
Trametinib
D
Cerulein (17d)
D1
D7
D17
shMEK1/2
E
Cxcl1
Tnfa
P = .0539
Ccl2
P = .0101
Icam1
P = .0028
Il1a
P = 0.0009
Il-16
P < .0001
Il-23
Cxcl12
P = .0056
No Dox
Dox
F
Insult
Acinar cell MAPK activation
Acinar to ductal metaplasia
Cytokine production
Inflammation / Fibrosis
necrosis-fibrosis sequence
MEK inhibition
Resolution?

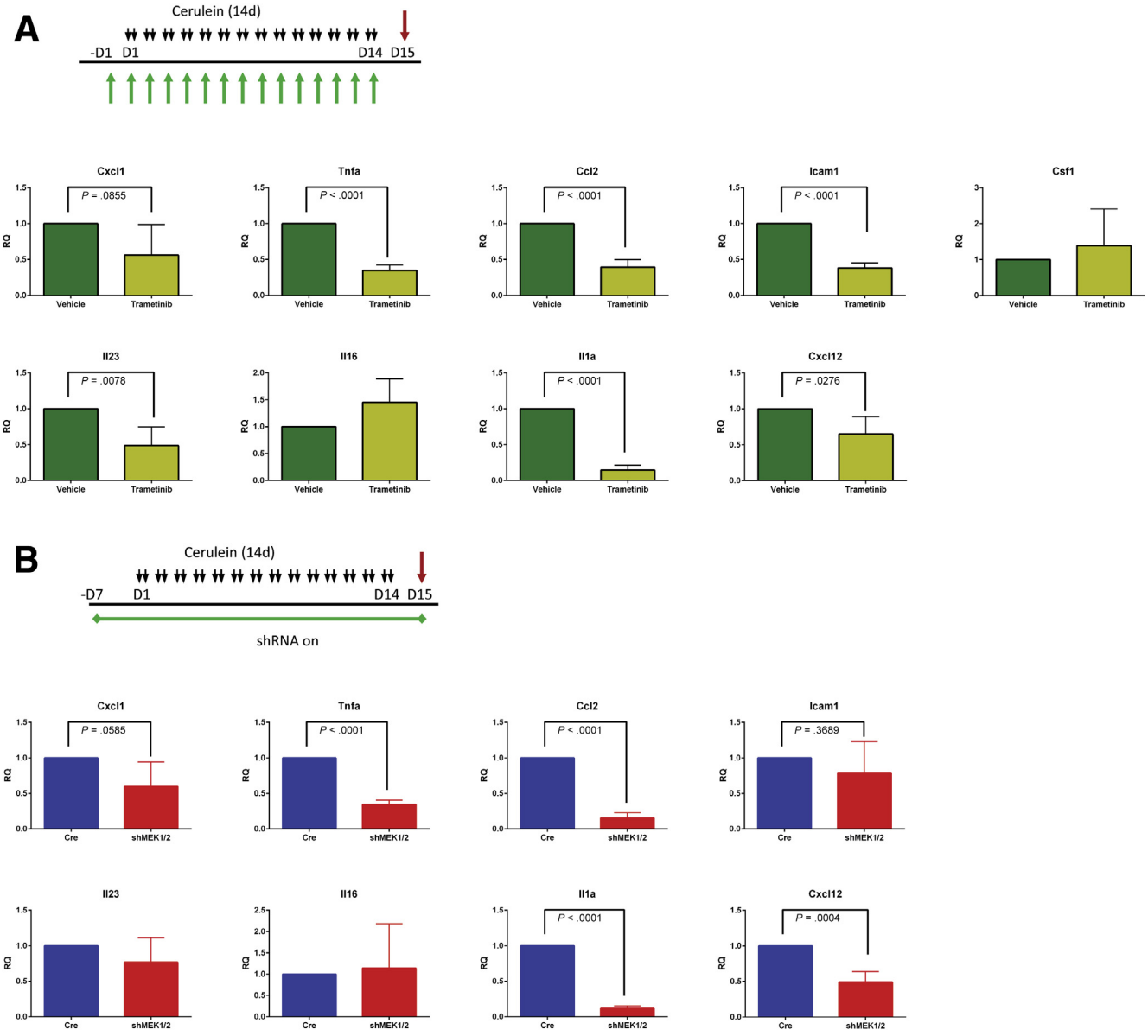

Figure 11. MEK inhibition prevents expression of inflammatory cytokines. (*A*) Schematic representation of CP protocol with inhibitor or vehicle treatment and qRT-PCR analysis of inflammatory cytokines from treated pancreata. (*B*) Schematic representation of CP protocol after initiation of shRNA expression in shMEK1/2 compared with Ptf1a$^{+/Cre}$ controls (Cre) and qRT-PCR analysis of cytokine expression in treated pancreata. Quantitation of respective staining for each group; error bars represent mean with standard deviation, n = 3 for all groups.

Cerulein-induced Pancreatitis, Doxycycline, and Inhibitor Treatments

Cerulein (American Peptide Company Inc, Sunnyvale, CA) was dissolved in sterile saline. For chronic pancreatitis, cerulein was administered to mice twice a day at a concentration of 250 μg/kg body weight via intraperitoneal injection. For acute pancreatitis, mice were given hourly injections of cerulein for 7 hours at a concentration of 50 μg/kg body weight and then killed after an hour of recovery. An equal volume of sterile saline was injected as a control.

Figure 10. (***See previous page***). MEK inhibition diminishes levels of inflammatory cytokines during pancreatitis. (*A*) CP protocol with drug pretreatment. (*B*) Immunoblot array of cytokines present in pancreata or untreated mice or mice treated with cerulein and either vehicle or trametinib. (*C*) qRT-PCR analysis of inflammatory cytokines present in pancreata treated with cerulein and vehicle or trametinib. (*D*) CP protocol (No Dox) or shRNA activation during CP protocol (Dox). (*E*) qRT-PCR analysis of inflammatory cytokines present in cerulein with or without doxycycline-induced shMEK1/2. (*F*) Potential mechanism of amelioration of CP by MEK inhibition.

Trametinib was injected intraperitoneally (Selleck Chemicals, Houston, TX) at 1 mg/kg and prepared as previously described.[44] BrdU (Sigma-Aldrich, St Louis, MO) was prepared in saline and injected intraperitoneally at 50 mg/kg 4 hours before death of the animal. Doxycycline was administered via chow at 200 mg doxycycline per kg of diet (Bio-Serv, Flemington, NJ).

Histology

Mice were killed by CO_2 asphyxiation; then tissue was quickly harvested and fixed overnight at room temperature with Z-fix solution (Anatech LTD, Battle Creek, MI). Tissues were processed by using a Leica (Buffalo Grove, IL) ASP300S Tissue Processor, paraffin embedded, and cut into 5-μm sections. Immunohistochemistry was performed on a Dako Autostainer Plus (Dako North America, Inc, Carpinteria, CA) or Discovery Ultra XT autostainer (Ventana Medical Systems Inc, Tucson, AZ) and counterstaining with hematoxylin. Dual immunohistochemistry for CK19 and amylase was performed without counterstaining. Picrosirius red staining was performed per the manufacturer's instructions (Polysciences, Inc, Warrington, PA). Hematoxylin-eosin staining was performed by using Mayer's hematoxylin solution (Sigma-Aldrich) and Eosin Y (Fisher, Pittsburgh, PA). Immunofluorescence was performed as previously described.[45] Immunohistochemistry slides were scanned on a Pannoramic SCAN slide scanner (Perkin Elmer, WA), and then annotation regions encompassing greater than 1 mm of tissue were processed by using appropriate algorithms for each stain quantified by using Halo software (Indica Labs, Corrales, NM). Immunofluorescence was quantified by manual counting of 5 fields per slide from images obtained on a Nikon A-1 confocal instrument at ×60 by using NIS-Elements software (Nikon Instruments, Melville, NY).

Antibodies

The antibodies used in this study are listed in Table 1.

RNA and Protein Harvest From Tissue

Mouse pancreas tissue lysate was obtained by quickly removing a piece of the pancreas from mice killed by CO_2 asphyxiation and snap freezing in liquid nitrogen. The frozen tissue was then homogenized in either RLT+ buffer for RNA or RIPA buffer supplemented with ethylenediamine tetraacetic acid–free protease inhibitor and PhosSTOP phosphatase inhibitor (Roche, South San Francisco, CA) by using a Pro 250 Homogenizer (Pro Scientific Inc, Oxford, CT). Lysate was then cleared by centrifugation and stored at −80°C. RNA was processed by using an RNEasy Plus kit (Qiagen, Valencia, CA) following the manufacturer's protocol.

Western Blotting

Lysates were quantified by BCA assay (Thermo Fisher Scientific Inc, Waltham, MA), and equal protein amounts were run onto sodium dodecylsulfate–polyacrylamide gel electrophoresis gels. Proteins were transferred from sodium dodecylsulfate–polyacrylamide gel electrophoresis gels to Immobilon-FL polyvinylidene difluoride membrane, blocked, and then incubated with primary antibodies. After washing, membranes were then incubated in secondary antibody, washed, and then exposed on autoradiography film (Bioexpress, Kaysville, UT) with West Pico ECL

Table 1. Antibodies Used in This Study

Antibody	Company	Catalog no.	Host species	Application
Amylase	Sigma-Aldrich	A8273	Rabbit	IHC
Anti-RFP	Life Technologies	R10367	Rabbit	IHC
BrdU	Abcam	ab3626	Rat	IHC
CD3	Abcam	ab5690	Rabbit	IHC
CK19	Develop. Studies Hybridoma Bank	Troma-III	Rat	IHC, IF
CPA1	R&D Systems	af2765	Mouse	IF
F4/80	ABD Serotec	MCA497G	Rat	IHC
HSP90	Cell Signaling	4874s	Rabbit	WB
Ki67	Vector Labs	VP-RM04	Rabbit	IF
Ly-6B.2	ABD Serotec	MCA771G	Rat	IHC
MEK1	Santa Cruz Biotechnology	SC219	Rabbit	WB
MEK2 (N-term)	Santa Cruz Biotechnology	sc524	Rabbit	WB
Turbo-GFP	Thermo Fisher Scientific	PA5-22688	Rabbit	IHC, WB
β-actin	Santa Cruz Biotechnology	sc-47778	Mouse	WB
p42/44 MAPK	Cell Signalling	9102	Rabbit	WB
p42/44 MAPK (T202/Y204)	Cell Signaling	4370P	Rabbit	WB

IF, immunofluorescence; IHC, immunohistochemistry; WB, Western Blot.

(Thermo Fisher Scientific Inc) or scanned on an Odyssey CLx scanner (LI-COR, Lincoln, NE). Quantitation of Western blots was performed by using ImageJ (National Institutes of Health, Bethesda, MD).

Serum Amylase Assay

Mice were killed by CO_2 asphyxiation, and blood was immediately harvested by cardiac puncture. Serum was separated by centrifugation in Microtainer vials containing a serum separation polymer (BD, Franklin Lakes, NJ). A kinetic amylase assay was then performed on a Synergy plate reader (BioTek, Winooski, VT) by using an amylase detection reagent according to the manufacturer's protocol (Pointe Scientific, Canton, MI).

Whole Animal Imaging

Fluorescence imaging was conducted by using an IVIS Spectrum (Perkin Elmer, Akron, OH) by using GFP filters.

Mouse Cytokine Array

Tissue lysate was prepared as above, and 100 μg protein from 2 mice of each treatment group was combined and analyzed by the mouse cytokine array panel as per the manufacturer's instructions (R&D Systems, Minneapolis, MN).

cDNA Synthesis and Quantitative Polymerase Chain Reaction

The cDNA was synthesized from isolated RNA with an iScript cDNA synthesis kit (BioRad, Hercules, CA). Quantitative PCR reactions were carried out with FastSyber master mix on a Viia7 thermocycler (Life Technologies, Grand Island, NY). Primer sets used for qPCR are listed in Table 2.

Three-dimensional Acinar Cell Explant Culture

The acinar cell isolation protocol has been previously described.[46] Briefly, the pancreas was harvested and minced with sterile scissors, digested with Collagenase P (Roche), passed through polypropylene mesh (Spectrum Laboratories, Rancho Dominguez, CA), and then pelleted through an fetal bovine serum gradient. The pelleted cells were embedded in growth factor reduced Matrigel, cultured with complete Waymouth's MB 752/1 medium (Sigma-Aldrich), and maintained at 37°C in 5% CO_2 atmosphere. The shRNA and Ptf1a$^{+/Cre}$ explant cultures were treated with 10 μg/mL doxycycline hyclate (Sigma-Aldrich). WT acinar explants were treated with 100 nmol/L trametinib or dimethyl sulfoxide. After 3 days (Ptf1a$^{+/Cre}$ and shRNA mice) or 5 days (WT mice) of culture, the ratio of acinar to ductal conversion was counted by a blinded observer as an average of ten ×20 fields on a CKX41 light microscope (Olympus, Waltham, MA).

Statistical Analysis

Statistics were performed by using Graph Pad Prism 6 (Graph Pad Software Inc, La Jolla, CA) by using an unpaired Student t test for comparison between 2 groups or a one-way analysis of variance with Tukey multiple comparison test.

Table 2. Sets of Primers Used in This Study

Gene	Direction	Primer
Hprt1	5'	TCAGTCAACGGGGGACATAAA
Hprt1	3'	GGGGCTGTACTGCTTAACCAG
Tbp	5'	CCCCACAACTCTTCCATTCT
Tbp	3'	GCAGGAGTGATAGGGGTCAT
Il1a	5'	CAAGATGGCCAAAGTTCCTGAC
Il1a	3'	GTCTCATGAAGTGAGCCATAGC
Cxcl12	5'	AGCCAACGTCAAGCATCTGA
Cxcl12	3'	CTTGCATCTCCCACGGATGT
Icam1	5'	TCCGCTGTGCTTTGAGAACT
Icam1	3'	GGCTCAGTATCTCCTCCCCA
Il-23	5'	TGGTTGTGACCCACAAGGAC
Il-23	3'	ATCCTCTGGCTGGAGGAGTT
Cxcl1	5'	CCGAAGTCATAGCCACACTCA
Cxcl1	3'	TTCACCAGACAGGTGCCATC
Ptf1a	5'	CATCGAGGCACCCGTTCAC
Ptf1a	3'	CAACCCGATGTGAGCTGTCT
Il16	5'	ACTTCCAGTGCATCTCAGGC
Il16	3'	CGGATGTCGGCTTACGATGA
Amy2b	5'	AGGAACATGGTTGCCTTCAG
Amy2b	3'	CTGACAAAGCCCAGTCATCA
Ck19	5'	CGCGGTGGAAGTTTTAGTGGG
Ck19	3'	AGGCGAGCATTGTCAATCTGTA
Mist1	5'	CTCGAATCCCCAGTTGGAAGG
Mist1	3'	CTCCGGAGACCCTTTGTCAG
Tnfa	5'	GACGTGGAACTGGCAGAAGAG
Tnfa	3'	TTGGTGGTTTGTGAGTGTGAG
Csf1	5'	GGTGGCTTTAGGGTACAGG
Csf1	3'	GACTTCATGCCAGATTGCC
Ccl2	5'	GGCTCAGCCAGATGCAGTTA
Ccl2	3'	GGACCCATTCCTTCTTGGGG

References

1. Yadav D, Lowenfels AB. The epidemiology of pancreatitis and pancreatic cancer. Gastroenterology 2013; 144:1252–1261.
2. Witt H, Apte MV, Keim V, et al. Chronic pancreatitis: challenges and advances in pathogenesis, genetics, diagnosis, and therapy. Gastroenterology 2007; 132:1557–1573.
3. Bhatia M, Brady M, Shokuhi S, et al. Inflammatory mediators in acute pancreatitis. J Pathol 2000;190:117–125.
4. Strobel O, Dor Y, Alsina J, et al. In vivo lineage tracing defines the role of acinar-to-ductal transdifferentiation in inflammatory ductal metaplasia. Gastroenterology 2007; 133:1999–2009.
5. Desai BM, Oliver-Krasinski J, De Leon DD, et al. Preexisting pancreatic acinar cells contribute to acinar cell, but

not islet beta cell, regeneration. J Clin Invest 2007; 117:971–977.
6. Fendrich V, Esni F, Garay MVR, et al. Hedgehog signaling is required for effective regeneration of exocrine pancreas. Gastroenterology 2008;135:621–631.
7. Ferreira MJ, McKenna LB, Zhang J, et al. Spontaneous pancreatitis caused by tissue-specific gene ablation of Hhex in mice. Cell Mol Gastroenterol Hepatol 2015; 1:550–569.
8. Liou GY, Doppler H, Necela B, et al. Macrophage-secreted cytokines drive pancreatic acinar-to-ductal metaplasia through NF-kappaB and MMPs. J Cell Biol 2013;202:563–577.
9. Huang H, Liu Y, Daniluk J, et al. Activation of nuclear factor-kappaB in acinar cells increases the severity of pancreatitis in mice. Gastroenterology 2013; 144:202–210.
10. Miyamoto Y, Maitra A, Ghosh B, et al. Notch mediates TGF alpha-induced changes in epithelial differentiation during pancreatic tumorigenesis. Cancer Cell 2003;3:565–576.
11. Sawey ET, Johnson JA, Crawford HC. Matrix metalloproteinase 7 controls pancreatic acinar cell transdifferentiation by activating the Notch signaling pathway. Proc Natl Acad Sci U S A 2007;104:19327–19332.
12. Means AL, Ray KC, Singh AB, et al. Overexpression of heparin-binding EGF-like growth factor in mouse pancreas results in fibrosis and epithelial metaplasia. Gastroenterology 2003;124:1020–1036.
13. Sandgren EP, Luetteke NC, Palmiter RD, et al. Overexpression of TGF alpha in transgenic mice: induction of epithelial hyperplasia, pancreatic metaplasia, and carcinoma of the breast. Cell 1990;61:1121–1135.
14. Ji BA, Tsou L, Wang HM, et al. Ras activity levels control the development of pancreatic diseases. Gastroenterology 2009;137:1072–1082.
15. Daniluk J, Liu Y, Deng DF, et al. An NF-kappa B pathway-mediated positive feedback loop amplifies Ras activity to pathological levels in mice. J Clin Invest 2012; 122:1519–1528.
16. Navas C, Hernandez-Porras I, Schuhmacher AJ, et al. EGF receptor signaling is essential for K-Ras oncogene-driven pancreatic ductal adenocarcinoma. Cancer Cell 2012;22:318–330.
17. Ardito CM, Gruner BM, Takeuchi KK, et al. EGF receptor is required for KRAS-induced pancreatic tumorigenesis. Cancer Cell 2012;22:304–317.
18. Collins MA, Yan W, Sebolt-Leopold JS, et al. MAPK signaling is required for dedifferentiation of acinar cells and development of pancreatic intraepithelial neoplasia in mice. Gastroenterology 2014;146:822–834.e7.
19. Xue J, Sharma V, Hsieh MH, et al. Alternatively activated macrophages promote pancreatic fibrosis in chronic pancreatitis. Nature Communications 2015;6:7158.
20. Belanger LF, Roy S, Tremblay M, et al. Mek2 is dispensable for mouse growth and development. Mol Cell Biol 2003;23:4778–4787.
21. Voisin L, Julien C, Duhamel S, et al. Activation of MEK1 or MEK2 isoform is sufficient to fully transform intestinal epithelial cells and induce the formation of metastatic tumors. BMC Cancer 2008;8:337.
22. Scholl FA, Dumesic PA, Barragan DI, et al. Mek1/2 gene dosage determines tissue response to oncogenic Ras signaling in the skin. Oncogene 2009;28:1485–1495.
23. Scholl FA, Dumesic PA, Barragan DI, et al. Selective role for Mek1 but not Mek2 in the induction of epidermal neoplasia. Cancer Res 2009;69:3772–3778.
24. Gailhouste L, Ezan F, Bessard A, et al. RNAi-mediated MEK1 knock-down prevents ERK1/2 activation and abolishes human hepatocarcinoma growth in vitro and in vivo. Int J Cancer 2010;126:1367–1377.
25. Lee CS, Dykema KJ, Hawkins DM, et al. MEK2 is sufficient but not necessary for proliferation and anchorage-independent growth of SK-MEL-28 melanoma cells. PLoS One 2011;6:e17165.
26. Mazzon E, Impellizzeri D, Di Paola R, et al. Effects of mitogen-activated protein kinase signaling pathway inhibition on the development of cerulein-induced acute pancreatitis in mice. Pancreas 2012;41:560–570.
27. Choi E, Hendley AM, Bailey JM, et al. Expression of activated Ras in gastric chief cells of mice leads to the full spectrum of metaplastic lineage transitions. Gastroenterology 2016;150:918–930 e13.
28. Pin CL, Bonvissuto AC, Konieczny SF. Mist1 expression is a common link among serous exocrine cells exhibiting regulated exocytosis. Anat Rec 2000;259:157–167.
29. Holtz BJ, Lodewyk KB, Sebolt-Leopold JS, et al. ERK activation is required for CCK-mediated pancreatic adaptive growth in mice. Am J Physiol Gastrointest Liver Physiol 2014;307:G700–G710.
30. Morisset J, Aliaga JC, Calvo EL, et al. Expression and modulation of p42/p44 MAPKs and cell cycle regulatory proteins in rat pancreas regeneration. Am J Physiol Gastrointest Liver Physiol 1999;277:G953–G959.
31. Pai R, Ohta M, Itani RM, et al. Induction of mitogen-activated protein kinase signal transduction pathway during gastric ulcer healing in rats. Gastroenterology 1998;114:706–713.
32. Jones MK, Tomikawa M, Mohajer B, et al. Gastrointestinal mucosal regeneration: role of growth factors. Front Biosci 1999;4:D303–D309.
33. El-Assal ON, Besner GE. HB-EGF enhances restitution after intestinal ischemia/reperfusion via PI3K/Akt and MEK/ERK1/2 activation. Gastroenterology 2005; 129:609–625.
34. Jiang HQ, Grenley MO, Bravo MJ, et al. EGFR/Ras/MAPK signaling mediates adult midgut epithelial homeostasis and regeneration in Drosophila. Cell Stem Cell 2011;8:84–95.
35. Wang CH, Guo XT, Xi RW. EGFR and Notch signaling respectively regulate proliferative activity and multiple cell lineage differentiation of Drosophila gastric stem cells. Cell Res 2014;24:610–627.
36. Rovira M, Scott SG, Liss AS, et al. Isolation and characterization of centroacinar/terminal ductal progenitor cells in adult mouse pancreas. Proc Natl Acad Sci U S A 2010;107:75–80.
37. Criscimanna A, Speicher JA, Houshmand G, et al. Duct cells contribute to regeneration of endocrine and acinar cells following pancreatic damage in adult mice. Gastroenterology 2011;141:1451–1462, e1–e6.

38. Strobel O, Rosow DE, Rakhlin EY, et al. Pancreatic duct glands are distinct ductal compartments that react to chronic injury and mediate shh-induced metaplasia. Gastroenterology 2010;138:1166–1177.
39. Westphalen CB, Takemoto Y, Tanaka T, et al. Dclk1 defines quiescent pancreatic progenitors that promote injury-induced regeneration and tumorigenesis. Cell Stem Cell 2016;18:441–455.
40. Criscimanna A, Coudriet GM, Gittes GK, et al. Activated macrophages create lineage-specific microenvironments for pancreatic acinar- and beta-cell regeneration in mice. Gastroenterology 2014;147:1106–1118.e11.
41. Premsrirut PK, Dow LE, Kim SY, et al. A rapid and scalable system for studying gene function in mice using conditional RNA interference. Cell 2011; 145:145–158.
42. Kawaguchi Y, Cooper B, Gannon M, et al. The role of the transcriptional regulator Ptf1a in converting intestinal to pancreatic progenitors. Nat Genet 2002; 32:128–134.
43. Saborowski M, Saborowski A, Morris JPt, et al. A modular and flexible ESC-based mouse model of pancreatic cancer. Genes Dev 2014;28:85–97.
44. Mazur PK, Reynoird N, Khatri P, et al. SMYD3 links lysine methylation of MAP3K2 to Ras-driven cancer. Nature 2014;510:283–287.
45. Collins MA, Bednar F, Zhang YQ, et al. Oncogenic Kras is required for both the initiation and maintenance of pancreatic cancer in mice. J Clin Invest 2012; 122:639–653.
46. Wu CYC, Carpenter ES, Takeuchi KK, et al. PI3K regulation of RAC1 is required for KRAS-induced pancreatic tumorigenesis in mice. Gastroenterology 2014; 147:1405–1416.e7.

Received July 29, 2016. Accepted September 17, 2016.

Reprint requests
Address requests for reprints to: Howard Crawford, PhD, NCRC Building 520, Room 1347, 1600 Huron Parkway, Ann Arbor, Michigan 48109-1600. e-mail: howcraw@umich.edu; fax: (734) 647-6977.

Acknowledgments
The authors thank Devon F. Pendlebury for assistance with mouse experiments, Brandy Edenfield and Daniel Long for assistance with histology, and Megan T. Hoffman for helpful discussion and scientific insight relating to this project. The TROMA-III monoclonal antibody to CK19 developed by R. Kemler was obtained from the Developmental Studies Hybridoma Bank developed under the auspices of the NICHD and maintained by the University of Iowa, Department of Biology, Iowa City, IA.

Conflicts of interest
The authors disclose no conflicts.

Funding
Supported by National Institutes of Health grants R01 CA159222 to H.C.C. and R01 CA151588 to M.P.M.